The Electronics of CH Activation by Energy Decomposition Analysis: From Transition Metals to Main-Group Metals

Clinton R. King, Samantha J. Gustafson, and Daniel H. Ess

Abstract Alkane CH activation is a fundamental reaction class where a metal-ligand complex reacts with a CH bond to give a metal-alkyl organometallic intermediate. CH activation reactions have been reported for a variety of transition metals and main-group metals. This chapter highlights recent quantum-mechanical studies that have used energy decomposition analysis (EDA) to provide insight into σ-coordination complexes and transition states for alkane CH activation reactions. These studies have provided new conceptual understanding of CH activation reactions and detailed insight into the physical nature and magnitude of interaction between alkanes with transition metals and main-group metals.

Keywords CH activation · Energy decomposition analysis · Transition metals · Main-group metals

Contents

C.R. King, S.J. Gustafson, and D.H. Ess (✉)
Department of Chemistry and Biochemistry, Brigham Young University,
Provo, UT 84602, USA
e-mail: dhe@chem.byu.edu

Scheme 1 General CH
bond functionalization
strategy

<div style="text-align:center">

CH Activation Rxn

$$MX + CH_4 \longrightarrow M-CH_3 + HX$$

MR Functionalization Rxn

$$M-CH_3 + 2HX + Ox \longrightarrow MX + CH_3X + H_2Ox$$

</div>

1 Introduction

CH activation reactions now play a dominant role in organometallic transformations and in synthetic organic reaction development [1–16]. In the context of this chapter, CH activation involves the reaction of a metal-ligand complex (MX) with an alkane CH bond to give an organometallic metal-alkyl (MR) intermediate that is hopefully more susceptible to substitution at carbon than the starting CH bond (Scheme 1) [17–20]. Generally, this CH bond functionalization strategy couples CH activation with a MR functionalization reaction where the organometallic intermediate is transformed into a partially oxidized alkane product. This two-step reaction sequence of CH activation and MR functionalization distinguishes this strategy from direct CH bond functionalization by metal oxo complexes or electrophilic organic reagents such as dioxiranes.

As experimental studies continue to discover new CH activation reactions, theory will play several significant roles such as (1) clarify and predict CH activation reaction mechanisms, (2) quantitatively predict CH activation transition-state barrier heights for new metal-ligand complexes, and (3) provide conceptual analysis of key CH activation intermediates and transition states. This last effort is the concern of this chapter and is important because conceptual analysis leads to understanding current reactivity and selectivity models and development of new models for the purpose of reaction discovery. Here we highlight select theoretical studies that have used energy decomposition analysis (EDA) methods to provide insight into intermediates and transition states for alkane CH activation reactions. Examples are discussed that provide detailed insight into the physical nature and magnitude of interaction of alkanes with transition metals and main-group metals. Nearly all examples discussed in this chapter have a direct relationship to experimental metal-ligand complexes that induce CH activation reactions.

2 Energy Decomposition Methods to Analyze CH Activation

There are several theoretical schemes to analyze the electronic structure of intermediates and transition states along a reaction pathway. Methods range from analysis of bonding using electron densities such as Bader's atoms-in-molecules

[21, 22] to second-order perturbation methods in natural bond orbital (NBO) analysis [23]. A particularly appealing method is EDA because this type of scheme relates the total energy of interaction (ΔE_{INT}) between two reacting molecules to mathematically well-defined and chemically meaningful types of interactions such as electrostatic energy, electron-electron repulsion energy, and electron delocalization energy. While there is no unique way to partition the energy of interaction between two molecules, the following provides a brief tutorial of how some of the most utilized EDA schemes dissect the interaction energy between reacting molecules. There are several excellent in-depth reviews of EDA methods and their application to chemical problems [24–31].

As two molecules react to form an intermediate or transition state, there are associated geometry changes and intramolecular and intermolecular electronic reorganization. For example, along the potential energy surface for CH activation of methane by a metal-ligand complex, there is CH bond stretching and alkane angle changes (Scheme 2). The metal-ligand complex also alters its geometry to accommodate the interaction with methane. This geometry change can be subtle if ligand rearrangement is unneeded but can be significant if, for example, a κ^2 ligand must transform into a κ^1 ligand. The energy associated with the difference in geometries between separated, noninteracting fragments and the reaction complex is called the distortion or activation-strain energy (ΔE_{DIST}, Eq. 1). The interaction between distorted fragments and the resulting energy stabilization is called the total interaction energy (ΔE_{INT}). The interaction energy between the distorted fragments controls the progress of geometric deformation required by the reactants to achieve the specific transition-state structure. The sum of the distortion and interaction energies gives the total energy of the bimolecular complex. For a transition-state structure, the sum of distortion and interaction energies is the activation energy:

Scheme 2 Relationship between distortion and interaction energies
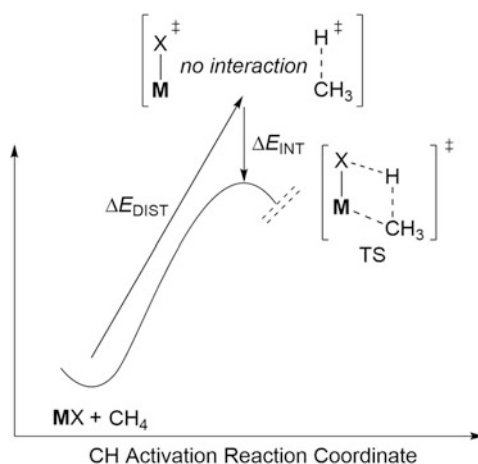
$$\Delta E = \Delta E_{\text{DIST}} + \Delta E_{\text{INT}} \tag{1}$$

While there are several insightful studies that analyze distortion energies [27, 29–31], this chapter emphasizes interaction energies and its dissection into specific physical terms. This dissection can be done in several different styles. Most EDA methods partition the interaction energy into components related to the classic frontier molecular orbital perturbation approach [32–36]. For example, the EDA method implemented in the Amsterdam Density Functional (ADF) program [24, 28, 37] partitions the interaction energy into contributions from electrostatic interactions (ΔE_{ELSTAT}), closed-shell or Pauli repulsion (ΔE_{PAULI}), and occupied-unoccupied orbital interactions (ΔE_{ORB}) (Eq. 2). Electrostatic interactions occur between nuclei-nuclei, nuclei-electron, and electron-electron. Closed-shell repulsion between interacting fragments arises from the requirement that same-spin electrons obey the Pauli exclusion principle. One way closed-shell repulsion is represented is by a classic 4-electron, 2-orbital interaction diagram shown on the left-hand side of Scheme 3. This diagram illustrates the net repulsion that occurs by having both bonding and antibonding orbitals filled. Delocalization orbital interactions result from the interaction of occupied and vacant orbitals. This is due to both intramolecular polarization and intermolecular interactions that describe electron delocalization. This latter type of occupied-vacant orbital interaction is described by the 2-electron, 2-orbital interaction diagram shown on the right-hand side of Scheme 3. This describes the energy stabilization resulting from partial electron density delocalization from the fragment with the occupied orbital to the fragment with the unoccupied orbital:

$$\Delta E_{\text{INT}} = \Delta E_{\text{ELSTAT}} + \Delta E_{\text{PAULI}} + \Delta E_{\text{ORB}} \tag{2}$$

While Eq. (2) represents the EDA method implemented in ADF, which is later referred to as ADF-EDA, there are several other implementations of EDA. One
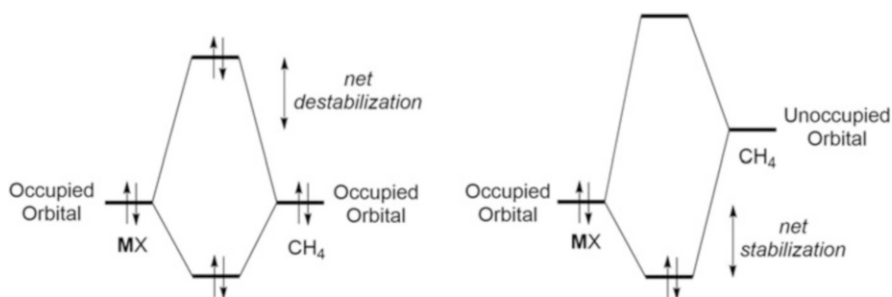
Scheme 3 Graphical illustration of Pauli repulsion (*left*) and occupied-unoccupied orbital stabilization upon charge transfer (*right*)

particularly useful method is the absolutely localized molecular orbital EDA (ALMO-EDA) [38, 39]. The ALMO-EDA method collapses the ΔE_{PAULI} and ΔE_{ELSTAT} terms into a single term that is called a frozen density term (ΔE_{FRZ}) Eq. (3). More importantly, the ALMO-EDA is a variational method that utilizes block localization of fragment molecular orbital coefficients to obtain directional intermolecular orbital stabilization, which is also labeled as charge transfer (ΔE_{CT}) stabilization (Eq. 4). Another advantage of the ALMO-EDA scheme is that this directional intermolecular orbital energy stabilization is separated from intramolecular orbital polarization stabilization (ΔE_{POL}). The orbital polarization stabilization is best related to intramolecular occupied-vacant orbital interactions that occur when one fragment is in the presence of the other fragment:

$$\Delta E_{INT} = \Delta E_{FRZ} + \Delta E_{POL} + \Delta E_{CT} \qquad (3)$$

$$\Delta E_{CT} = \Delta E_{CT1} + \Delta E_{CT2} \qquad (4)$$

The intermolecular orbital stabilization energy term, ΔE_{CT}, provides an estimate of all occupied-to-unoccupied orbital interactions between distorted fragments. However, the energy stabilization is often dominated by the interaction between the highest occupied and lowest unoccupied molecular orbitals (HOMO and LUMO) of each distorted fragment (Scheme 3). For CH activation reactions, the orbital interactions corresponding to electron delocalization from the metal-ligand complex to the alkane corresponds to back-bonding, ΔE_{CT1} (Scheme 4). The orbital interactions/electron delocalization from the alkane to the metal-ligand complex and the forward-bonding energy stabilization is ΔE_{CT2}. The sum of the back-bonding and forward-bonding intermolecular orbital interaction stabilization approximately gives the total intermolecular orbital stabilization energy in Eq. (4).

Scheme 4 Qualitative frontier orbital interactions that correspond to the back-bonding and forward-bonding electron delocalization
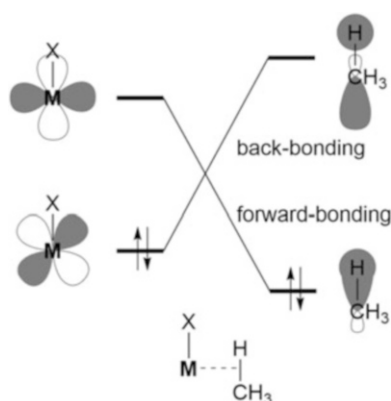
3 The Electronics of Alkane CH Bond Coordination

The CH activation reaction often occurs in two steps: (1) alkane coordination and (2) CH bond cleavage (Scheme 5). However, there are several examples of single-step reaction mechanisms. An alkane coordination complex (or σ-complex) involves the direct interaction of one or more alkane CH bonds with the inner sphere of the transition metal. There are now several examples of direct experimental detection of alkane complexes [40–42]. From a modeling perspective, an alkane coordination complex is an energy minimum structure on the potential energy landscape. Quantum-mechanical methods have been critical in characterizing these complexes and their energies, which can require accurate treatment of dispersion and spin-orbital coupling energies [43]. Alkane complexes are often exothermic (5–15 kcal/mol) relative to the starting metal-ligand complex and alkane if the metal has a vacant coordination site. However, alkane complexes are often endothermic relative to the starting metal-ligand complex and alkane if the metal is saturated with ligands and requires ligand dissociation prior to alkane inner-sphere contact with the metal center. Conceptually, the CH bond-metal interaction of an alkane complex involves both back-bonding and forward-bonding orbital interactions along with other intermolecular interactions. EDA provides a method to examine the chemical/physical driving force for interaction between the CH bond and the metal center. Historically, the stability of metal-alkane complexes has been attributed to back-bonding orbital interactions, and this is thought to be critical for strong interactions [1–16].

Bergman, Head-Gordon, and coworkers used the ALMO-EDA scheme to analyze the origin of alkane coordination to an experimentally relevant $CpRe(CO)_2$ complex [44]. As discussed earlier, the ALMO-EDA method is advantageous because it directly determines the relative amounts of forward-bonding and back-bonding orbital interactions in the context of their quantitative contribution to the total interaction energy. Scheme 6 shows how the EDA fragments were defined and

CH Activation Process

$$MX + CH_4 \xrightarrow{\text{Step 1. Alkane Coordination}} [M(CH_4)]^+ + X^- \xrightarrow{\text{Step 2. CH Bond Cleavage}} M{-}CH_3 + HX$$
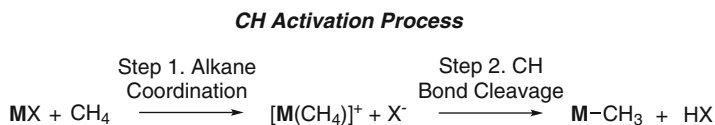
Scheme 5 Two-step reaction sequence for CH activation

Energy: methane (heptane)
ΔE_{INT} = -13.8 (-15.4)
ΔE_{FRZ} = 12.3 (13.1)
ΔE_{POL} = -4.4 (-5.2)
ΔE_{CT} = -21.7 (-23.3)
% ΔE_{CT1} = 26% (24%)
% ΔE_{CT2} = 74% (76%)
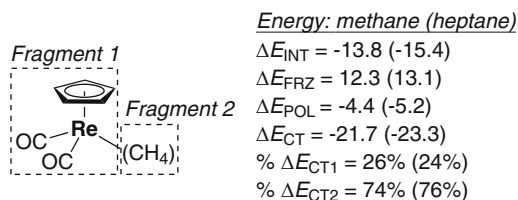
Scheme 6 BP86 ALMO-EDA energies reported by Cobar et al. [44] (kcal/mol)

the BP86 ALMO-EDA results reported by Bergman, Head-Gordon, and coworkers for the alkane complex interaction energies (ΔE_{INT}) of methane and heptane with $CpRe(CO)_2$. The total DFT interaction energies compare very well to experimental estimates.

The ALMO-EDA results in Scheme 6 reveal two interesting features of alkane coordination energy. First, the largest portion of the stabilizing interaction energy results from charge transfer as a result of orbital interactions. For example, the ΔE_{CT} energy stabilization for methane is -21.7 kcal/mol while ΔE_{POL} stabilization is only -4.4 kcal/mol. Second, in contrast to traditional concepts, the majority of alkane orbital stabilization energy ($\sim$75%) is the result of forward-bonding orbital interactions. Back-bonding orbital interactions are responsible for only $\sim$25% of the orbital stabilization energy. This suggests that while the dominant interaction that stabilizes alkane complexes is the forward-bonding orbital interaction shown in Scheme 4, non-negligible back-bonding interactions also occur. The relative magnitude of back-bonding and forward-bonding orbital stabilization energies is reminiscent to that found in many metal-H_2 complexes.

Our group has also used the ALMO-EDA scheme to analyze methane complexes that are related to Ir, Ru, Os, and Rh metal-ligand complexes that are known to experimentally promote CH bond activation [45]. These metal-ligand complexes differ from $CpRe(CO)_2$ in that a ligand must be displaced prior to coordination. Therefore, EDA was performed on the alkane coordination complexes as well as the transition states en route to alkane coordination. Scheme 7 shows an example of the results reported for methane coordination to $(acac)_2Ir(OAc)$ via an associative coordination transition state. Similar to the results for the $CpRe(CO)_2(CH_4)$ complex, the energy stabilization for the $(acac)_2Ir(OAc)(CH_4)$ complex results mainly from forward-bonding orbital interactions. Despite the significant difference in ligand architecture, metal center, oxidation state, and endothermic alkane coordination, the forward-bonding interaction is responsible for $\sim$80% of the orbital interaction stabilization energy while back-bonding is responsible for only $\sim$20%
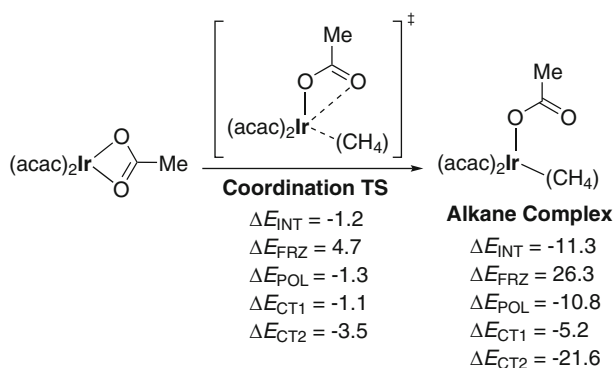
Scheme 7 B3LYP ALMO-EDA energies reported by Ess and coworkers [45]. EDA fragments were defined as $(acac)_2Ir(OAc)$ and CH_4 (acac = acetylacetonate, kcal/mol)

of orbital stabilization energy. However, inspection of the ALMO-EDA values for the coordination transition state reveals a very different description of the interaction of methane with the metal center and its ligands. Overall, there is only a very small interaction energy, and this suggests that the transition-state barrier for alkane coordination is dominated by acetate ligand dissociation to create a vacant coordination site for methane to approach and interact with the Ir metal center, and repulsion and stabilizing interactions are very weak between Ir and methane.

Another EDA study that was reported by our group focused on CH bond activation by Ir and Rh methyl, hydroxyl, and amido complexes with acac and Tp ligands [46]. For $(acac)_2IrX$, where $X = CH_3$ and OH, a methane coordination complex was identified on the potential energy surface. No minimum energy structure was located for the $(acac)_2IrNH_2$ complex. Similar results were found for the TpRu(CO)X complexes. Use of the ALMO-EDA method revealed that regardless of whether $X = CH_3$ or NH_2, the relative components to the interaction energy are similar. This report also highlighted that the ALMO-EDA scheme is relatively insensitive to the specific density functional used. B3LYP and M06 density functionals gave nearly identical results.

As an alternative to using EDA calculations to analyze back-bonding and forward-bonding orbital interactions, NBO-type calculations can also be used. The details of NBO calculations can be found elsewhere [23]. NBO analysis of donor-acceptor orbital interactions can be advantageous because the interpretation using localized orbitals and their interactions parallel the simplistic orbital interaction diagram shown in Scheme 4. However, the drawback of NBO calculations in the context of analyzing metal-alkane complexes is that estimates of back-bonding and forward-bonding orbital interactions are often not quantitatively directly related to the total interaction energy. Most of the time, the upside of NBO analysis outweighs its drawbacks and leads to useful conceptual understanding.

A recent example of NBO analysis of back-bonding and forward-bonding orbital interactions was performed on the $[(Cy_2PCH_2CH_2PCy_2)Rh(norbornane)]^+$ (Cy = cyclohexyl) alkane complex [47]. This alkane complex was directly detected by experiment in the solid state. Experiments and DFT calculations indicate that two CH bonds from one of the ethylene bridges of norbornane engage the Rh metal center. Similar to the ALMO-EDA results for the Re, Ir, and other alkane complexes, NBO analysis on $[(Cy_2PCH_2CH_2PCy_2)Rh(norbornane)]^+$ revealed that the major stabilizing interactions responsible for the stability of this alkane complex is forward-bonding interactions, which are approximately twice as stabilizing as back-bonding orbital interactions. In this instance, the key empty orbital on Rh is a Rh-P σ^* orbital that interacts with the filled CH σ orbitals. This interaction is twice as stabilizing as the sum of several filled Rh d_σ and Rh-P bonding orbitals interacting with the CH σ^* orbitals. Overall this and other NBO examples combined with the ALMO-EDA results suggest that for weakly interacting alkane complexes, the dominating stabilization is forward-bonding orbital interactions.

4 The Electronics of Alkane CH Bond Cleavage

Theory and experiment have identified a variety of CH bond cleavage mechanisms that result from either the alkane complex or directly from the metal-ligand complex and alkane [48, 49]. Because CH activation reactions have been discovered for many of the d-block transition metals, there has been a significant effort to classify and compare the mechanisms for CH bond cleavage. This is because often the specific choice of a metal and ligand results in a particular mechanism. Scheme 8 portrays oxidative addition and σ-bond metathesis mechanisms and their corresponding CH bond cleavage transition states, which represent the extremes of the commonly reported mechanisms. Intermediate between these extremes is a composite of the two transition states where the end result is a σ-bond metathesis mechanisms, but the metal is highly involved in bonding to the hydrogen in the transition state. This type of composite transition state has several names for nuanced versions, such as oxidatively added transition state (OATS) [50, 51], metal-assisted σ-bond metathesis (MAσBM) [52, 53], or σ-complex assisted metathesis (σ-CAM) [54]. Hall and Vastine [55] have shown that using atoms-in-molecules analysis provides a framework to understand the entire set of transition states along this mechanistic continuum.

Rather than focus on classifying CH activation reactions by mechanisms, our lab was interested in understanding and classifying the electronic reorganization that occurs in CH bond cleavage transition states as a possible tool to elucidate design principles for new CH activation reactions. Similar to the analysis of alkane coordination complexes, we used the EDA approach to probe the components of the interaction energy in the transition states. One potential advantage of an electronic reorganization viewpoint for classifying CH activation reactions is that many different metals and ligands can be analyzed without consideration of mechanism labels. Broadly, we considered two mechanisms labeled as insertion and substitution. Insertion transition states lead to a metal-hydride intermediate while substitution transition states pass the alkane hydrogen to a ligand. Scheme 9 shows insertion and substitution transition states and how EDA fragmentation was assigned.

In discussing electronic reorganization in the transition state, we have adopted the classic terms of electrophile and nucleophile that were previously used by Ryabov [56] for CH activation transition states. In the context of CH activation reactions, these terms are metal centric and refer to the overall influence of the
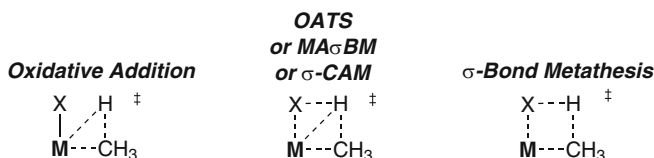
Scheme 8 Examples of mechanisms identified by theory and experiment for CH bond cleavage

Insertion TS   **Substitution TS**

$$\left[\begin{array}{c} X \quad \overset{\text{\textbraceleft}}{\underset{\text{\textbraceleft}}{\vdots}} \quad H \\ \Big| \diagup \quad \vdots \\ M - \overset{\text{\textbraceleft}}{\underset{\text{\textbraceleft}}{\vdots}} - CH_3 \end{array}\right]^{\ddagger} \qquad \left[\begin{array}{c} X - \overset{\text{\textbraceleft}}{\underset{\text{\textbraceleft}}{\vdots}} - H \\ \vdots \quad \vdots \\ M - \overset{\text{\textbraceleft}}{\underset{\text{\textbraceleft}}{\vdots}} - CH_3 \end{array}\right]^{\ddagger}$$

MX Fragment   CH Fragment   *MX Fragment   CH Fragment*

Scheme 9 Definition of EDA fragments for insertion and substitution transition states

metal-ligand fragment on the alkane. While there is no unique way to measure electrophilicity or nucleophilicity in a transition state, one useful approach is to estimate the energy stabilization resulting from electron delocalization due to orbital interactions. Outlined in Scheme 4, the simplified frontier orbital interactions that occur for alkane complexes also occur in CH bond cleavage transition states but are amplified. An electrophilic transition state is defined by a transition state where the majority of energy stabilization that occurs upon interaction between the metal-ligand and alkane results from forward-bonding orbital interactions. A nucleophilic transition state is defined by a transition state where the majority of energy stabilization that occurs upon interaction between the metal-ligand and alkane results from back-bonding orbital interactions. Whether back-bonding or forward-bonding orbital interactions dominate in the transition state is related to relative orbital energies of the metal-ligand complex and alkane and orbital overlap.

The ALMO-EDA scheme was used to analyze a wide range of methane CH bond cleavage transition states for metal-ligand complexes that have been reported experimentally to promote or catalyze CH activation [57]. This included late transition metals such as Rh(III), Rh(I), Ir(III), Pt(II), Pd(II), Ru(II), and Au(III) and early transition metals such as Sc(III) and W(II). Ligands attached to these metal centers range from phosphine, N-heterocycle, and halide to O-donors. Three specific examples of transition states analyzed and their ALMO-EDA interaction energy components are shown in Scheme 10.

This ALMO energy analysis revealed several important features about the nature of CH bond cleavage transition states: (1) By plotting the difference and ratio of ΔE_{CT1} and ΔE_{CT2} for the transition states, this revealed that there is a continuum from electrophilic to nucleophilic with several metal-ligand complexes that act as ambiphiles towards methane. The ΔE_{FRZ} and ΔE_{POL} energy terms were not considered in electrophilic/nucleophilic character assignment since these terms do not result from intermolecular electron delocalization. This continuum is illustrated in Scheme 10 by [(Hbpym)PtCl]$^{+2}$ that induces a transition state with methane where the dominant orbital stabilization energy results from forward-bonding (ΔE_{CT2}) and on the opposite extreme (PCP)Ir that induces a transition state with methane where the dominant orbital stabilization energy is back-bonding (ΔE_{CT1}). (2) Insertion and substitution-type mechanisms were found for electrophilic, ambiphilic, and nucleophilic transition states. (3) Terms such as oxidative addition do not imply electronic changes in the transition state. For example, the label oxidative addition is often used for insertion reactions between Pt(II) and alkanes. However, for
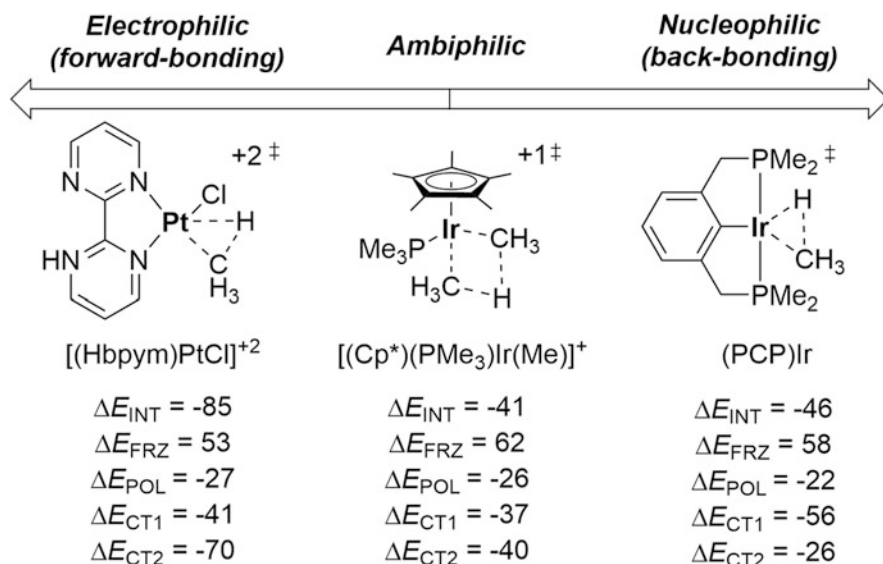
Scheme 10 Examples of electrophilic, ambiphilic, and nucleophilic metal-ligand complexes [57] (kcal/mol)

[(Hbpym)PtCl]$^{+2}$ reacting with methane, the oxidative addition transition state is electrophilic and dominated by donation of electron density from methane to Pt. In contrast, the (PCP)Ir complex induces oxidative addition with the main orbital energy stabilization to the transition state interaction energy involving electron density delocalization from (PCP)Ir to methane. (4) Although there was no quantitative correlation between the relative ALMO-EDA charge transfer energy stabilization and frontier orbital energy gaps, transition-state fragment orbital energies were found to qualitatively reflect electrophilic, ambiphilic, or nucleophilic character.

Overall, late transition metals, such as Au(III), Rh(III), Pd(II), and Pt(II), with a variety of N-donor and O-donor ligands were often found to have electrophilic transition states. Ru(II) and Ir(III) with N-donor and O-donor ligands as well as [Cp*(PMe$_3$)IrMe]$^+$ were found to act in an ambiphilic manner towards methane. Despite substitution-type transition states having both a Lewis acid metal and a Lewis base ligand that interacts with the CH bond of methane, these transition states are not always ambiphilic. For example, in the transition state between d^0 (Cp*)$_2$ScMe and methane, the (Cp*)$_2$ScMe complex acts as a nucleophile. Other nucleophilic transition states involved methane reaction with W(II), Ir(I), and Rh (I) complexes.

An ab initio molecular dynamics (AIMD) study by Vidossich, Ujaque, and Lledós examined the reaction pathway for methane reacting with Cl$_2$Pd(H$_2$O) [58]. This study verified that this and similar Pt(II) complexes act as electrophiles towards methane. Along the reaction pathway and at the Cl$_2$Pd(H$_2$O)(H)

Scheme 11 Comparison of ALMO-EDA and ADF-EDA results for the CH activation cleavage transition state between $CsNH_2$ and methane (kcal/mol)

<div align="center">

Substitution TS

H_2N - - -H   ‡

Cs - -CH_3

</div>

B3LYP **ALMO-EDA**	**BLYP** **ADF-EDA**
$\Delta E_{INT} = -26.5$	$\Delta E_{INT} = -25.4$
$\Delta E_{FRZ} = 73.7$	$\Delta E_{PAULI} = 147.2$
$\Delta E_{POL} = -48.7$	$\Delta E_{ESTAT} = -77.9$
$\Delta E_{CT1} = -49.2$	$\Delta E_{ORB} = -94.7$
$\Delta E_{CT2} = -2.3$	
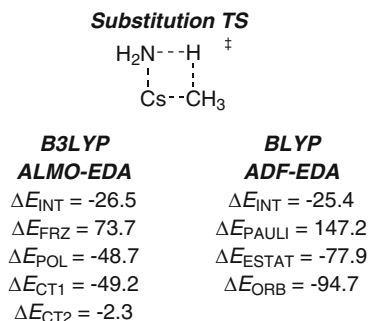
(Me) intermediate, maximally localized Wannier functions were used to analyze the oxidation state of Pt. These localized bonding functions indicate that the Pt metal center remains Pt(II) throughout the reaction pathway without significant oxidation, which is in line with a highly electrophilic CH activation process.

To further examine the nucleophilic side of the CH activation continuum, the our group and the Cundari group undertook a computational study [59] of alkali metal amide and alkaline earth metal amide CH activation reactions with alkanes. This study is directly related to classic superbase chemistry using cesium cyclohexylamide-type reagents to induce CH bond deprotonation of alkanes [60].

While simple model systems using a single metal amide complex were used, this study illustrates a few important points. Scheme 11 shows the results reported using ALMO-EDA and ADF-EDA to analyze the transition state between $CsNH_2$ and methane. Importantly, while these different EDA schemes have a high degree of compatibility, they provide different information. For example, the total interaction energies are within 1 kcal/mol, and the ΔE_{FRZ} term is very close to the sum of the ΔE_{ELSTAT} and ΔE_{PAULI} ADF-EDA terms. The B3LYP ΔE_{FRZ} energy is 73.7 kcal/mol while the sum of the BLYP ΔE_{ELSTAT} and ΔE_{PAULI} terms is 69.3 kcal/mol.

The B3LYP ALMO-EDA values confirm the expected highly nucleophilic character of this transition state, which is the result of the amide group interacting with the methane CH σ^* and results in -49.2 kcal/mol of stabilization energy. Forward-bonding due to the interaction between the methane σ CH bond and the Cs vacant orbital is only -2.3 kcal/mol stabilizing.

For highly nucleophilic (or electrophilic) transition states, it is important to also examine the interaction energy components where electrostatic interactions are separated from closed-shell (Pauli) repulsion energy. The ADF-EDA interaction energy values in Scheme 11 indicate that in the $CsNH_2$-methane transition state the interaction energy has nearly equal energy stabilization from orbital interactions and electrostatic interactions. This is important because highly polarized transition states are often assumed to have very little covalent (i.e., orbital) energy stabilization. The ALMO-EDA energy components also reveal that half of this orbital stabilization is due to intramolecular orbital polarization (ΔE_{POL}) and half is due to electron delocalization (ΔE_{CT}). This illustrates that in general very polar transition states with significant electrostatic stabilization will induce a large amount of

Scheme 12 Comparison of ADF-EDA results reported by Bickelhaupt and coworkers for methane insertion by Pd(0) and Ca (0) [61–64] (kcal/mol)

Insertion TS

$$Pd \overset{\diagup H}{\underset{\diagdown CH_3}{\cdots}}^{\ddagger} \qquad Ca \overset{\diagup H}{\underset{\diagdown CH_3}{\cdots}}^{\ddagger}$$

BLYP ADF-EDA

$\Delta E_{INT} = -48.3$
$\Delta E_{PAULI} = 201.7$
$\Delta E_{ESTAT} = -159.1$
$\Delta E_{ORB} = -90.9$

BLYP ADF-EDA

$\Delta E_{INT} = -23.0$
$\Delta E_{PAULI} = 164.9$
$\Delta E_{ESTAT} = -83.5$
$\Delta E_{ORB} = -104.4$
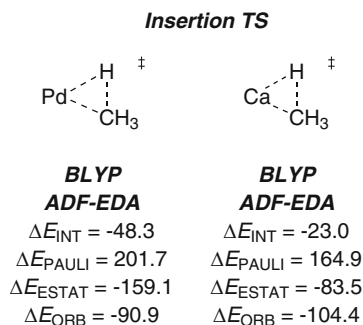
intramolecular polarization energy stabilization. Overall, this study showed that the combination of using the ALMO-EDA and ADF-EDA methods provides a unified and insightful view of highly polarized CH activation transition states.

The Bickelhaupt group has applied the ADF-EDA scheme to a number of model alkane CH activation reactions (for select examples, see [61–64]). In one report, insertion transition states were analyzed for model CH activation reactions between methane and zero-valent group 2 (Be, Mg, and Ca) and group 12 (Zn and Cd) metals [61–64]. One motivation of this study was to provide an understanding based on transition state interactions why the lowest oxidation state of s-block main-group elements compared to Pd(0) have dramatically larger activation barriers for methane CH bond insertion. However, more relevant to this discussion is that the ADF-EDA given in Scheme 12 provide insight into the differences in transition-state electronic reorganization for s-block versus transition-metal elements for CH bond cleavage of methane. Surprisingly, in the Ca transition state, there is a nearly equal amount of electrostatic and orbital stabilization, while in the Pd transition state the electrostatics dominate the stabilizing interaction energy.

The Bickelhaupt group also examined model CH activation reactions between methane and low-oxidation state group-11 transition-metal cations Cu(I), Ag(I), and Au(I), with a comparison to Pd(0) [61–64]. This study revealed that at the beginning of the reaction pathway the low-oxidation state group II cations are more effective electrophiles than Pd(0) due to the much lower energy of the 4s, 5s, or 6s LUMOs. However, as the reaction progresses towards the transition state, back-bonding interactions become more important, and the group II cations are less effective at back-bonding compared to Pd(0).

Recently, the Periana group disclosed that main-group Tl(III) and Pb (IV) trifluoroacetate metal-ligand complexes promote alkane partial oxidation, and our group showed that this occurs via a CH activation mechanism (Scheme 13) [65]. While the above discussion has highlighted insights about the electronic character of CH activation reactions for transition-metal complexes, there is relatively little known about the electronic character for CH activation by p-block main-group metals. The ALMO-EDA and ADF-EDA component energies for the rate-limiting transition state between Tl(TFA)$_3$ and methane are reported in Scheme 13.
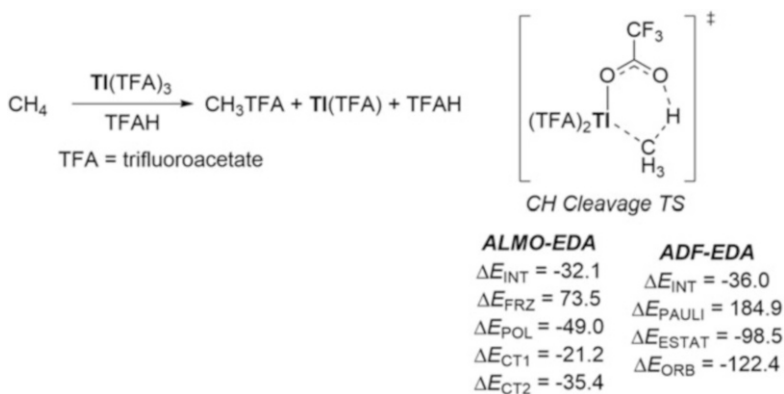
Scheme 13 Tl(III)-promoted methane CH activation transition state and ALMO-EDA (M06/6-31 + G(d,p)[LANL2DZ]) and ADF-EDA (BP86/TZ2P-ZORA) component energies (kcal/mol)

Comparison of ΔE_{CT1} and ΔE_{CT2} indicate, as expected, that Tl(III) acts as a relatively strong electrophile towards methane with the main orbital stabilization energy resulting from forward-bonding orbital interactions in the transition state. While orbital interactions provide the largest ALMO-EDA stabilization energy to the total interaction energy, polarization stabilization energy is nearly as significant in magnitude. Because the polarization energy stabilization is large, it is important to also examine the ADF-EDA values that analyze electrostatic stabilization. The ADF-EDA values reported in Scheme 13 indicate that orbital energy stabilization is larger than electrostatic stabilization, but when polarization is considered from the ALMO-EDA the transition state is nearly equally comprised of stabilization from charge transfer and electrostatic interactions.

5   Conclusions

The theoretical studies highlighted here used EDA to provide detailed insights into the physical interactions that occur along the reaction pathway for CH activation. Use of the ALMO-EDA scheme revealed that weak alkane complexes form primarily as a result of forward-bonding orbital interactions. In contrast, transition states that involve CH bond cleavage can either be dominated by forward-bonding or back-bonding interactions, which are, respectively, referred to as electrophilic and nucleophilic transition states. There are also transition states that have nearly equal energy stabilization from forward-bonding or back-bonding interactions. While many details are known about the electronic reorganization during CH activation by transition metals, there is relatively little known about CH activation reactions with main-group metals. EDA applied to the Tl(III)-methane CH activation transition state revealed that Tl(III) reacts as a strong electrophile and that there is nearly equal energy stabilization from orbital interactions and electrostatic interactions.

References

1. Crabtree RH (1985) Chem Rev 85:245
2. Shilov AE, Shul'pin GB (1987) Russ Chem Rev 56:442
3. Arndtsen BA, Bergman RG (1995) Science 270:1970
4. Crabtree RH (1995) Chem Rev 95:987
5. Shilov AE, Shul'pin GB (1997) Chem Rev 97:2879
6. Stahl SS, Labinger JA, Bercaw JE (1998) Angew Chem Int Ed 37:2180
7. Crabtree RH (2001) J Chem Soc Dalton Trans 2437
8. Labinger JA, Bercaw JE (2002) Nature 417:507
9. Ritleng V, Sirlin C, Pfeffer M (2002) Chem Rev 102:1731
10. Jones WD (2003) Acc Chem Res 36:140
11. Goldman AS, Goldberg KI (2004) Organometallic C–H bond activation: an introduction. In: Goldman AS, Goldberg KI (eds) Activation and functionalization of C–H bonds, vol 885, ACS symposium series. Wiley, Washington, p 1
12. Crabtree RH (2004) J Organomet Chem 689:4083
13. Labinger JA (2004) J Mol Catal A Chem 220:27
14. Hashiguchi BG, Hövelmann CH, Bischof SM, Lokare KS, Leung CH, Periana RA (2010) Methane-to-methanol conversion. In: Crabtree RH (ed) Energy production and storage: inorganic chemical strategies for a warming world, Encyclopedia of inorganic chemistry. Wiley, Chichester, p 101
15. Gunnoe TB (2012) In: Perez PJ (ed) Alkane C–H activation by single-site metal catalysts, vol. 38. Springer, Dordrecht, pp 1–15
16. Cavaliere VN, Wicker BF, Mindiola DJ (2012) Adv Organomet Chem 60:1
17. Conley BL, Tenn WJ III, Young KJH, Ganesh SK, Meier SK, Ziatdinov VR, Mironov O, Oxgaard J, Gonzales J, Goddard WA III, Periana RA (2006) J Mol Catal A 251:8
18. Webb JR, Bolaño T, Gunnoe TB (2011) ChemSusChem 4:37
19. Golisz SR, Gunnoe TB, Goddard WA III, Groves JR, Periana RA (2011) Catal Lett 141:213
20. Hashiguchi BG, Bischof SM, Konnick MM, Periana RA (2012) Acc Chem Res 45:885
21. Bader R (1990) Atoms in molecules: a quantum theory. Oxford University Press, New York
22. Popelier PLA (2014) The QTAIM perspective of chemical bonding. In The chemical bond. Wiley-VCH , Weinheim, pp 271–308
23. Weinhold F, Landis CR (2012) Discovering chemistry with natural bond orbitals. Wiley, Hoboken
24. Bickelhaupt FM, Baerends EJ (2000) Kohn-sham DFT: predicting and understanding chemistry. In: Boyd DB, Lipkowitz KB (eds) Reviews in computational chemistry, vol 15. Wiley-VCH, New York, pp 1–86
25. von Hopffgarten M, Frenking G (2012) WIREs Comput Mol Sci 2:43
26. Lein M, Frenking G (2005) The nature of the chemical bond in the light of an energy decomposition analysis. In: Dykstra CE, Frenking G, Kim KS, Scuseria GE (eds) Theory and applications of computational chemistry: the first forty years. Elsevier , Amsterdam, pp 291–372
27. van Zeist WJ, Bickelhaupt FM (2010) Org Biomol Chem 8:3118
28. Frenking G, Bickelhaupt FM (2014) The EDA perspective of chemical bonding. In: Frenking G, Shaik S (eds) The chemical bond. Wiley-VCH, Weinheim, pp 121–157
29. Fernández I (2014) Phys Chem Chem Phys 16:7662
30. Fernández I, Bickelhaupt FM (2014) Chem Soc Rev 43:4953
31. Fernández I (2014) Understanding trends in reaction barriers. In: Pignataro B (ed) Discovering the future of molecular sciences. Wiley-VCH, Weinheim, pp 165–187
32. Klopman G (1968) J Am Chem Soc 90:223
33. Salem L (1968) J Am Chem Soc 90:543
34. Salem L (1968) J Am Chem Soc 90:553
35. Morokuma K (1971) J Chem Phys 55:1236

36. Ziegler T, Rauk A (1977) Theor Chim Acta 46:1
37. ADF (2014) SCM theoretical chemistry. Vrije Universiteit, Amsterdam. http://www.scm.com
38. Khaliullin RZ, Cobar EA, Lochan RC, Bell AT, Head-Gordon M (2007) J Phys Chem A 111:8753
39. Khaliullin RZ, Bell AT, Head-Gordon M (2008) J Chem Phys 128:184112
40. Walter MD, White PS, Schauer CK, Brookhart M (2013) J Am Chem Soc 135:15933
41. Pike SD, Thompson AL, Algarra AG, Apperley DC, Macgregor SA, Weller AS (2012) Science 337:1648
42. Bernskoetter WH, Schauer CK, Goldberg KI, Brookhart M (2009) Science 326:553
43. Chan B, Ball GE (2013) J Chem Theory Comput 9:2199
44. Cobar EA, Khaliullin RZ, Bergman RG, Head-Gordon M (2007) Proc Nat Acad Sci USA 104:6963
45. Ess DH, Bischof SM, Oxgaard J, Periana RA, Goddard WA III (2008) Organometallics 27:6440
46. Ess DH, Gunnoe TB, Cundari TR, Goddard WA III, Periana RA (2010) Organometallics 29:6801
47. Pike SD, Chadwick FM, Rees NH, Scott MP, Weller AS, Kramer T, Macgregor SA (2015) J Am Chem Soc 137:820
48. Balcells D, Clot E, Eisenstein O (2010) Chem Rev 110:749
49. Ackermann L (2011) Chem Rev 111:1315
50. Ng SM, Lam WH, Mak CC, Tsang CW, Jia G, Lin Z, Lau CP (2003) Organometallics 22:641
51. Lam WH, Jia G, Lin Z, Lau CP, Eisenstein O (2003) Chem Eur J 9:2775
52. Webster CE, Fan Y, Hall MB, Kunz D, Hartwig JF (2003) J Am Chem Soc 125:858
53. Hartwig JF, Cook KS, Hapke M, Incarvito CD, Fan Y, Webster CE, Hall MB (2005) J Am Chem Soc 127:2538
54. Perutz RN, Sabo-Etienne S (2007) Angew Chem Int Ed 46:2578
55. Vastine BA, Hall MB (2007) J Am Chem Soc 129:12068
56. Ryabov AD (1990) Chem Rev 90:403
57. Ess DH, Goddard WA III, Periana RA (2010) Organometallics 29:6459
58. Vidossich P, Ujaque G, Lledós A (2012) Chem Commun 48:1979
59. Pardue DB, Gustafson SJ, Periana RA, Ess DH, Cundari TR (2013) Comput Theor Chem 1019:85
60. Streitwieser A Jr, Ciuffarin E, Hammons JH (1967) J Am Chem Soc 89:63
61. Diefenbach A, de Jong GT, Bickelhaupt FM (2005) J Chem Theory Comput 1:286
62. Wolters LP, van Zeist WJ, Bickelhaupt FM (2014) Chem Eur J 20:11370
63. de Jong GT, Visser R, Bickelhaupt FM (2006) J Organomet Chem 691:4341
64. de Jong GT, Bickelhaupt FM (2009) Can J Chem 87:806
65. Hashiguchi BG, Konnick MM, Bischof SM, Gustafson SJ, Devarajan D, Gunsalus N, Ess DH, Periana RA (2014) Science 343:1232